 Related Commentary, page 558

Behavioral stress accelerates prostate cancer development in mice

Sazzad Hassan,[1] Yelena Karpova,[1] Daniele Baiz,[1] Dana Yancey,[1] Ashok Pullikuth,[1] Anabel Flores,[1] Thomas Register,[2,3] J. Mark Cline,[2,3] Ralph D'Agostino Jr.,[3] Nika Danial,[4] Sandeep Robert Datta,[5] and George Kulik[1,3]

[1]Department of Cancer Biology, [2]Department of Pathology, and [3]Comprehensive Cancer Center, Wake Forest University School of Medicine, Winston-Salem, North Carolina, USA. [4]Department of Cancer Biology, Dana-Farber Cancer Institute, Boston, Massachusetts, USA. [5]Department of Neurobiology, Harvard Medical School, Boston, Massachusetts, USA.

Prostate cancer patients have increased levels of stress and anxiety. Conversely, men who take beta blockers, which interfere with signaling from the stress hormones adrenaline and noradrenaline, have a lower incidence of prostate cancer; however, the mechanisms underlying stress–prostate cancer interactions are unknown. Here, we report that stress promotes prostate carcinogenesis in mice in an adrenaline-dependent manner. Behavioral stress inhibited apoptosis and delayed prostate tumor involution both in phosphatase and tensin homolog–deficient (PTEN-deficient) prostate cancer xenografts treated with PI3K inhibitor and in prostate tumors of mice with prostate-restricted expression of c-MYC (Hi-Myc mice) subjected to androgen ablation therapy with bicalutamide. Additionally, stress accelerated prostate cancer development in Hi-Myc mice. The effects of stress were prevented by treatment with the selective β_2-adrenergic receptor (ADRB2) antagonist ICI118,551 or by inducible expression of PKA inhibitor (PKI) or of BCL2-associated death promoter (BAD) with a mutated PKA phosphorylation site (BAD^{S112A}) in xenograft tumors. Effects of stress were also blocked in Hi-Myc mice expressing phosphorylation-deficient BAD (BAD^{3SA}). These results demonstrate interactions between prostate tumors and the psychosocial environment mediated by activation of an adrenaline/ADRB2/PKA/BAD antiapoptotic signaling pathway. Our findings could be used to identify prostate cancer patients who could benefit from stress reduction or from pharmacological inhibition of stress-induced signaling.

Introduction

Substantial geographical variations in prostate cancer incidence in men with similar genetic backgrounds suggest that environmental factors are important in prostate cancer development (1). Several studies in prostate cancer patients have shown that changing to a low-fat, plant-based diet combined with stress management modulates gene expression and slows the rate at which levels of prostate-specific antigen (PSA) increase (2, 3). Curiously, although these studies included a stress reduction component to alleviate the stress of dietary changes, they did not examine the effects of the stress reduction per se on prostate cancer. Indeed, most attention so far has been focused on diet as the dominant environmental factor that influences cancer. Yet for higher organisms, psychosocial interactions could have a substantial effect on hormonal status and well being, as evidenced by reports that chronic stress and depression predict cancer progression and mortality (4, 5).

A cancer diagnosis itself is known to be a major distress factor, causing anxiety and depression (4), and patients with prostate cancer reportedly show higher levels of anxiety compared with other cancer patients (6). Furthermore, higher levels of PSA have been observed in patients under behavioral stress (7, 8), and increased stress levels have been connected with inflammatory prostatitis (9). Conversely, an 18% reduction of prostate cancer risk has been reported in patients who take beta blockers, which interfere with signaling of the stress hormones adrenaline and noradrenaline (10). Still, information is limited concerning mechanisms by which stress influences prostate cancer. Experiments in tissue culture models have shown that β_2-adrenergic receptor (ADRB2) activation inhibits apoptosis and stimulates migration, whereas glucocorticoid receptor activation inhibits proliferation, in prostate cancer cells (11–13). In vivo experiments showed that implanting nude mice with a noradrenaline-releasing micropump increased metastasis of PC3 xenografts by 1.6-fold (12). However, to date, there is no definitive experimental evidence on the mechanisms by which behavioral stress may influence prostate cancer development and therapy resistance.

Considering that increased stress and anxiety are common comorbidities for prostate cancer, we decided to test the effects of behavioral stress in vivo in mouse models of prostate cancer. We examined the effects of immobilization stress on therapeutic sensitivity of prostate cancer C42 xenografts in nude mice and on prostate tumors in mice with prostate-restricted expression of c-MYC (referred to herein as Hi-Myc mice). We report that the PI3K inhibitor ZSTK474 induced apoptosis in C42 prostate cancer xenografts, whereas subjecting mice to immobilization stress or to injection with adrenaline prevented ZSTK474-induced apoptosis and sustained tumor growth. Experiments with (a) ICI118,551, a selective antagonist of ADRB2; (b) inducible expression of the PKA inhibitor PKI-GFP; and (c) BCL2-associated death promoter (BAD) with a mutated PKA phosphorylation site at S112 delineated a dominant role of the ADRB2/PKA/BAD signaling pathway in apoptosis inhibition. The generality of this signaling mechanism was demonstrated by experiments with Hi-Myc mice. Immobilization stress induced BAD phosphorylation in prostates of these mice, inhibited apoptosis, and increased size of mouse prostatic intraepithelial neoplasia (PIN) and overall prostate weight compared with nonstressed mice. Stress also delayed prostate involu-

Conflict of interest: The authors have declared that no conflict of interest exists.
Citation for this article: *J Clin Invest.* 2013;123(2):874–886. doi:10.1172/JCI63324.

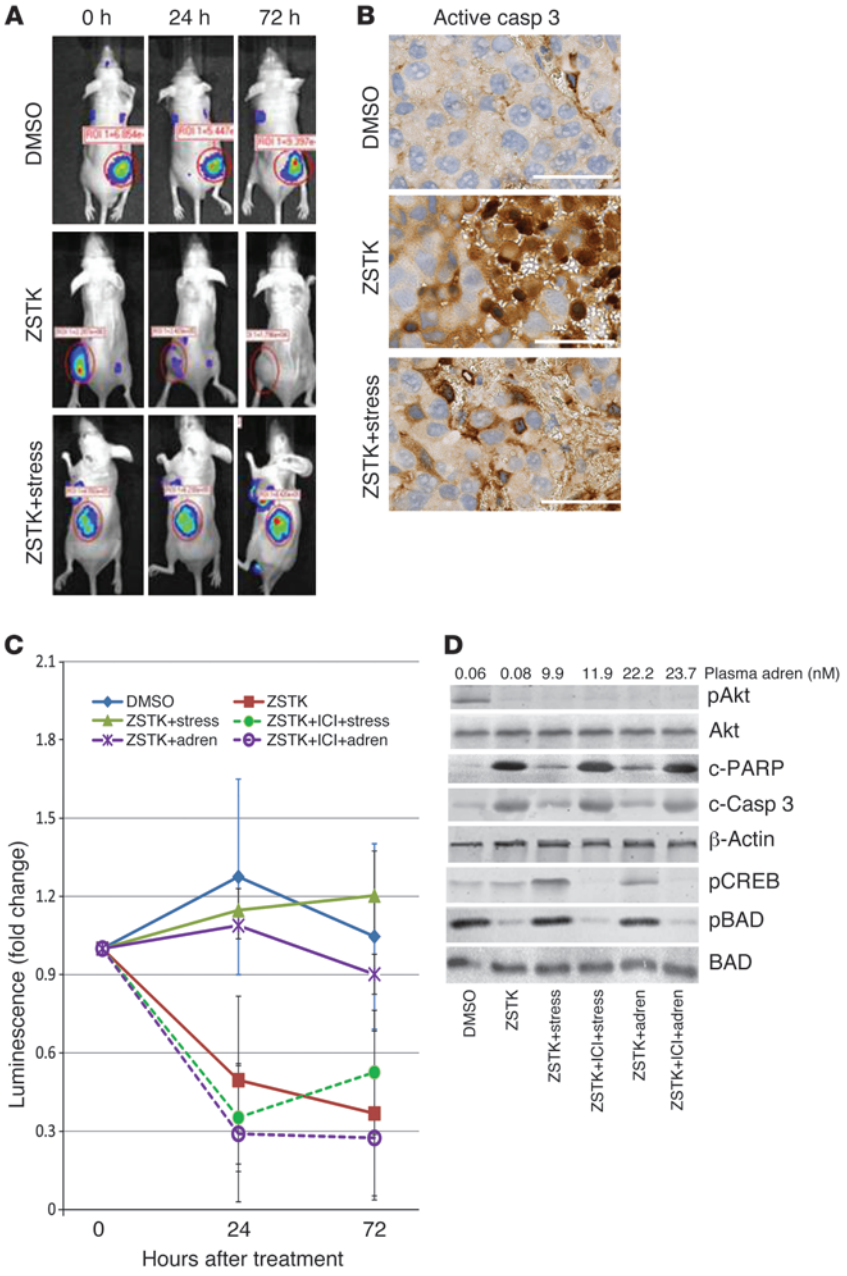

Figure 1
Stress or adrenaline prevents apoptosis induced by PI3K inhibitor in prostate cancer xenografts. (**A**) Representative images of mice with C42LucBAD xenografts. Mice were injected with DMSO, ZSTK474 (ZSTK), or ZSTK474 followed by immobilization stress. Luminescence of xenograft tumors was measured before injection of PI3K inhibitors (0 hour) and after injections at 24 and 72 hours. (**B**) Immunohistochemical analysis of cleaved caspase-3 in C42LucBAD xenograft tumors. Mice were treated as in **A**, and xenografts were excised 6 hours after injections. Scale bars: 50 μm. (**C**) Dynamics of luminescence in C42LucBAD xenograft tumors. Mice were injected with DMSO (n = 3), ZSTK474 (n = 3), ZSTK474 followed by immobilization stress (n = 3), ZSTK474 and adrenaline (adren; n = 3), ZSTK474 and ICI118,551 (ICI) followed by immobilization stress (n = 3), or ZSTK474, ICI118,551, and adrenaline (n = 4). Error bars show SD from the average of measurements in at least 3 mice. Comparisons between pairs of groups were performed using t tests derived from the overall ANOVA model. Significant between-group differences over time were as follows: $P < 0.02$, ZSTK vs. DMSO; $P < 0.01$, ZSTK+stress vs. ZSTK; $P < 0.03$, ZSTK+adren vs. ZSTK; $P < 0.003$, ZSTK+ICI+stress vs. ZSTK+stress; $P < 0.006$, ZSTK+ICI+adren vs. ZSTK+adren. (**D**) Western blot analysis of C42LucBAD xenograft tumor tissues excised 6 hours after injection of ZSTK474 and/or ICI118,551 (ICI) into mice that were then subjected to immobilization stress, left intact, or injected with epinephrine. At the time of xenograft excision, blood was collected for adrenaline measurements (shown above blots).

tion in mice subjected to androgen ablation therapy with bicalutamide (Casodex). Consistent with the role of the ADRB2/PKA/BAD signaling pathway, the effects of stress were blocked by providing Hi-Myc mice with ICI118,551 as well as in Hi-MycBAD$^{3SA/WT}$ mice, in which endogenous BAD was replaced with phosphorylation-deficient mutant BAD^{3SA} (14).

Results

Immobilization stress protects prostate cancer xenografts from apoptosis via adrenaline/ADRB2 signaling. To address the role of stress in therapeutic resistance of prostate cancer, we examined effects of immobilization stress on the responses of C42LucBAD xenografts to the PI3K inhibitor ZSTK474. Immobilization and exposure to predator scent is a well-established method of inducing behavioral stress in mice (15, 16). In our experiments, this technique increased adrenaline blood levels on average to 12 nM in stressed groups for at least 12 hours, whereas in nonstressed intact (or calm) mice, adrenaline was typically less than 1 nM (Supplemental Figure 1; supplemental material available online with this article; doi:10.1172/JCI63324DS1). Analysis of tumor tissue extracts also showed increased catecholamine levels in stressed mice (Supplemental Table 1).

C42 prostate cancer cells, which were used for xenograft studies, are among the best-characterized models of androgen-independent prostate cancer (17). The PI3K/AKT pathway is constitutively active in these cells due to the loss of tumor suppressor phosphatase and tensin homolog (PTEN), as is true for up to 70% of advanced androgen-independent prostate cancers (18). C42LucBAD cells were engineered to express firefly luciferase and

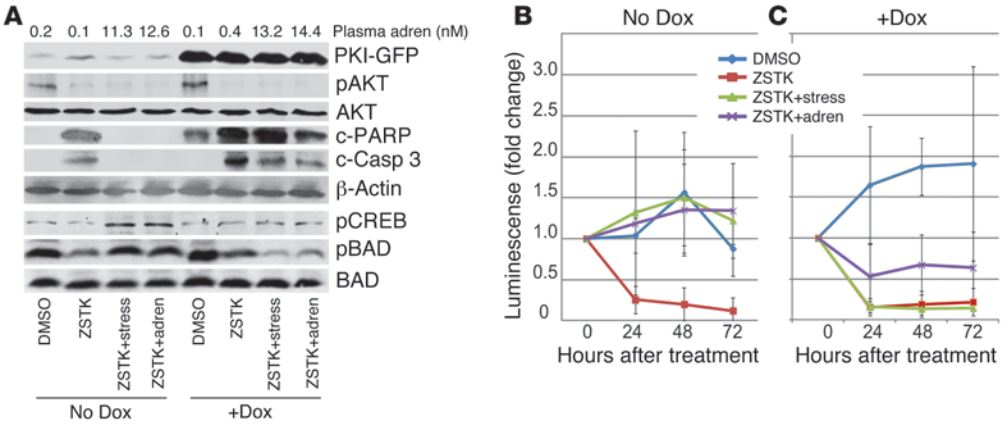

Figure 2

Activation of PKA is necessary for stress- or adrenaline-induced protection from apoptosis in prostate cancer xenografts. (**A**) Analysis of C42LucPKI xenograft tumors by Western blotting. ZSTK474 inhibited pAkt^{S473} and pBAD^{S112} and induced cleavage of PARP and caspase-3. Stress or adrenaline induced pBAD^{S112} and pCREB^{S133} and inhibited cleavage of PARP and caspase-3. These effects of stress or adrenaline were blocked by doxycycline-induced (Dox) PKI-GFP expression. At the time of tumor excision, blood was collected for adrenaline measurements (shown above blots). (**B** and **C**) Effects of stress and adrenaline on tumor luminescence depend on PKA activity. Mice were injected with DMSO as a control or with ZSTK474, with or without adrenaline or subsequent immobilization stress. Comparisons between groups were performed using *t* tests derived from the overall ANOVA model. (**B**) In mice that did not receive doxycycline, significant differences in luminescence across time were found in ZSTK+stress ($P < 0.0002$) and ZSTK+adren ($P < 0.0002$) groups versus ZSTK. (**C**) These differences were eliminated by doxycycline-induced PKI-GFP expression ($P > 0.63$ and $P > 0.13$, respectively). Error bars in **B** and **C** show the SD from the average of measurements in at least 4 mice.

HA-BAD. Expression of BAD provides a more uniform response of xenograft tumors to PI3K inhibitors, whereas luciferase expression allows noninvasive monitoring of xenograft tumors in mice in vivo by luminescent imaging.

Injection of the PI3K inhibitor ZSTK474 into C42LucBAD xenografts substantially reduced luminescence, as well as tumor volume (as measured by magnetic resonance imaging; Supplemental Figure 2), whereas subjecting mice to immobilization stress prevented this reduction of luminescence in C42LucBAD xenografts (Figure 1, A and C). Immunohistochemical analysis of tumor xenografts with antibodies that recognize active caspase-3 showed increased staining of prostate cancer cells in ZSTK474-injected xenografts; staining was decreased in xenografts from mice subjected to immobilization stress (Figure 1B). The validity of staining for active caspase-3 to identify apoptosis in C42LucBAD cells was confirmed by TUNEL; in most cases, staining for TUNEL and active caspase-3 overlapped (Supplemental Figure 3). Analysis of proteins extracted from tumor xenografts by Western blotting confirmed the appearance of the active cleaved form of caspase-3 and cleavage of the caspase substrate PARP in tumors with reduced luminescence (Figure 1D), whereas no changes in cleaved caspase-3 and PARP were observed in xenografts excised from stressed mice not injected with ZSTK474 (Supplemental Figure 4). Therefore, diminished luminescence of xenograft tumors reflects increased apoptosis of C42LucBAD cells.

Because beta blockers were reported to reduce prostate cancer incidence and mortality (10, 19), and ADRB2 is the predominant adrenergic receptor in LNCaP/C42 prostate cancer cells (20), we examined the effects of stress in the presence of the selective ADRB2 antagonist ICI118,551 (21). Effects of stress on xenograft luminescence and apoptosis (i.e., PARP and caspase-3 cleavage) were completely blocked by ICI118,551 (Figure 1, C and D). Conversely, injections of adrenaline mimicked the effects of stress on xenografts' luminescence and apoptosis. As was the case with stress, effects of adrenaline injections were blocked by ICI118,551 (Figure 1C). Taken together, our results suggest that adrenaline signaling via ADRB2 is necessary and sufficient to inhibit apoptosis in prostate cancer xenografts of mice subjected to immobilization stress.

Stress protects C42Luc xenografts from apoptosis via PKA/BAD^{S112} signaling. To examine signaling pathways that control apoptosis in prostate cancer xenografts, we targeted phosphorylation of BAD, a BH3-only proapoptotic member of the Bcl2 protein family. Earlier tissue culture experiments identified BAD as a convergence node for several survival signaling pathways in prostate cancer and breast cancer cells (22, 23). However, in vivo evidence that BAD phosphorylation plays a critical role in antiapoptotic signaling in prostate tumors has been lacking. BAD is continuously phosphorylated at S112, S136, and S155 in PTEN-deficient prostate cancer cells. Phosphorylation at either BAD^{S112} or BAD^{S136} facilitates binding to 14-3-3 proteins and neutralizes the proapoptotic properties of BAD (24). In prostate cancer cells, inhibition of PI3K led to dephosphorylation of BAD^{S112} and BAD^{S136} and increased apoptosis, while antiapoptotic signaling by vasoactive intestinal peptide, adrenaline, or the RAF/MAPK pathway restored phosphorylation of BAD^{S112} and inhibited apoptosis (11, 22).

ZSTK474 inhibited phosphorylated AKT^{S473} (pAKT^{S473}) and pBAD^{S112} in xenograft tumors of intact mice. However, in mice subjected to immobilization stress or injected with adrenaline, BAD phosphorylation was restored, despite continuous inhibition of the PI3K/AKT pathway (Figure 1D). Injection of ICI118,551 prevented BAD phosphorylation by either stress or adrenaline. Since C42Luc xenografts are characterized by constitutive activation of the PI3K pathway, BAD was constitutively phosphorylated. Its phosphorylation status was not changed significantly by stress in the absence of ZSTK474, although CREB phosphorylation was increased (Supplemental Figure 4). These results demonstrated that immobilization stress triggers PI3K/AKT-independent phosphorylation of BAD via the adrenaline/ADRB2 axis in prostate cancer xenografts.

PKA has been identified as one of the downstream effectors of ADRB2 signaling and as a BAD^{S112} kinase (25, 26). We thus analyzed phosphorylation of CREB^{S133}, an established PKA substrate (27), in prostate cancer xenografts; similar to BAD^{S112}, both stress and adrenaline stimulated pCREB^{S133}, and these effects were reversed by ICI118,551 (Figure 1D).

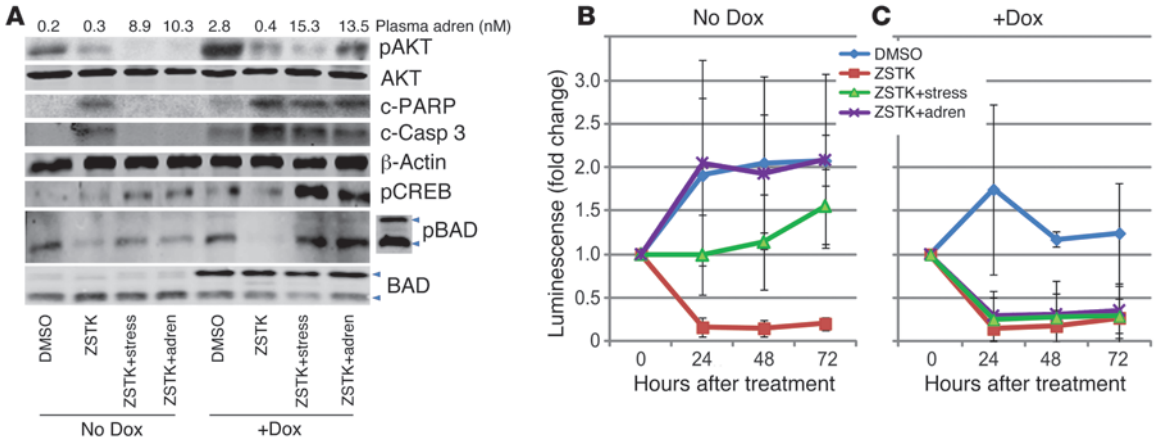

Figure 3

Activation of pBAD^{S112} is necessary for stress- or adrenaline-induced protection from apoptosis in prostate cancer xenografts. (**A**) Analysis of C42LucBAD^{1SA} xenograft tumors by Western blotting. ZSTK474 inhibited pAkt^{S473} and pBAD^{S112} and induced cleavage of PARP and caspase-3. Stress or adrenaline induced pBAD^{S112} and pCREB^{S133} and inhibited cleavage of PARP and caspase-3. Effects of stress or adrenaline on apoptosis (cleavage of caspase-3 and PARP) were blocked by doxycycline-induced expression of mutant HA-BAD^{S112A}. Arrowheads denote HA-BAD^{1SA} (top) and endogenous BAD (bottom). The inset at right from a pBAD blot shows lysates of C42LucBAD cells that served as positive control for phosphorylated HA-BAD. Mutant HA-BAD^{S112A} (lanes 5–7) could not be phosphorylated and was not recognized by pBAD^{S112}-specific antibodies. (**B** and **C**) Effects of stress or adrenaline on tumor luminescence depend on pBAD^{S112}. (**B**) In mice that did not receive doxycycline, luminescence in ZSTK+stress and ZSTK+adren groups was highly significantly different compared with the ZSTK group ($P < 0.0001$ for both). (**C**) These differences were completely eliminated by doxycycline-induced expression of pBAD^{S112}-deficient HA-BAD^{1SA} ($P > 0.65$ and $P > 0.52$, respectively). Error bars in **B** and **C** show the SD from the average of measurements in at least 4 mice.

To directly test the role of PKA in antiapoptotic signaling by stress or adrenaline in vivo, we generated C42LucPKI cells that inducibly express a chimera of the PKA inhibitor peptide PKI and GFP (PKI-GFP; ref. 28). Induction of PKI-GFP expression in C42LucPKI prostate cancer cells prevented adrenaline-induced activation of PKA to a degree similar to pretreatment with ICI118,551, as shown by lack of CREB phosphorylation (Supplemental Figure 5). Likewise, in subcutaneously implanted C42LucPKI xenografts, doxycycline-induced PKI-GFP expression prevented phosphorylation of the PKA substrates CREB^{S133} and BAD^{S112} in response to stress or adrenaline injection (Figure 2A). Furthermore, doxycycline-induced expression of GFP-PKI in C42Luc xenografts blocked the antiapoptotic effects of stress or adrenaline, as evidenced by the increased levels of cleaved caspase-3 and cleaved PARP.

Consistent with increased apoptosis, decreased luminescence was observed in C42LucPKI xenografts injected with ZSTK474 in mice that received doxycycline before stress or adrenaline injection, whereas in the absence of doxycycline, stress and adrenaline prevented the loss of luminescence in ZSTK474-injected xenograft tumors (Figure 2, B and C). Thus, inhibition of PKA rendered cancer cells insensitive to antiapoptotic signaling activated by adrenaline or by immobilization stress.

A similar strategy was used to test the role of pBAD^{S112} in antiapoptotic signaling by stress. We generated C42LucBAD^{1SA} cells that express BAD^{S122A} under a doxycycline-inducible promoter. In the absence of doxycycline, these xenograft tumors responded to injection of ZSTK474 by decreased luminescence; immobilization stress or injection of adrenaline reversed the effect of ZSTK474. Yet in xenografts with doxycycline-induced expression of mutant BAD^{S112A}, neither stress nor adrenaline restored luminescence in tumors injected with ZSTK474 (Figure 3). Consistent with these data, doxycycline-induced expression of BAD^{S112A} prevented inhibition of caspase-3 cleavage and PARP cleavage, despite increased phosphorylation of CREB, in response to stress or adrenaline. These results suggest that expression of the phosphorylation-deficient BAD mutant inhibits the antiapoptotic effects of stress or adrenaline downstream from PKA. In contrast, C42LucBAD xenografts that ectopically express WT BAD were protected from apoptosis by stress and by adrenaline (Figure 1). In summary, these results provide evidence that PKA-dependent BAD^{S112} phosphorylation plays a decisive role in antiapoptotic effects of stress in prostate xenograft tumors.

Behavioral stress activates adrenaline/ADRB2 signaling, inhibits apoptosis, and accelerates cancer development in mouse prostates. Experiments with subcutaneously implanted C42 xenografts demonstrated that psychosocial stress could activate the adrenaline/ADRB2/PKA/BAD antiapoptotic signaling pathway in prostate tumors that grow outside of prostate gland and boost their therapeutic resistance. However, these experiments did not elucidate whether stress could activate antiapoptotic mechanisms in the prostate. To address this question, we examined phosphorylation of the PKA substrates CREB and BAD in prostates of mice subjected to immobilization stress. pBAD^{S112} and pCREB^{S133} increased in prostates of stressed FVB or BALB/c nude mice (Figure 4A and Supplemental Figure 6A). Statistically significant positive correlations were observed between adrenaline levels and pBAD^{S112} and pCREB^{S133} in prostates of stressed mice (Supplemental Figure 6B).

These results suggest that an adrenaline/ADRB2/PKA/BAD antiapoptotic signaling pathway activated in response to behavioral stress could contribute to the progression of primary prostate tumors in mice. To test this hypothesis, we chose Hi-Myc mice, a model of prostate cancer driven by prostate-restricted expression of c-MYC under a probasin promoter (29). Ectopic expression of c-MYC increases both proliferation and apoptosis in various cell

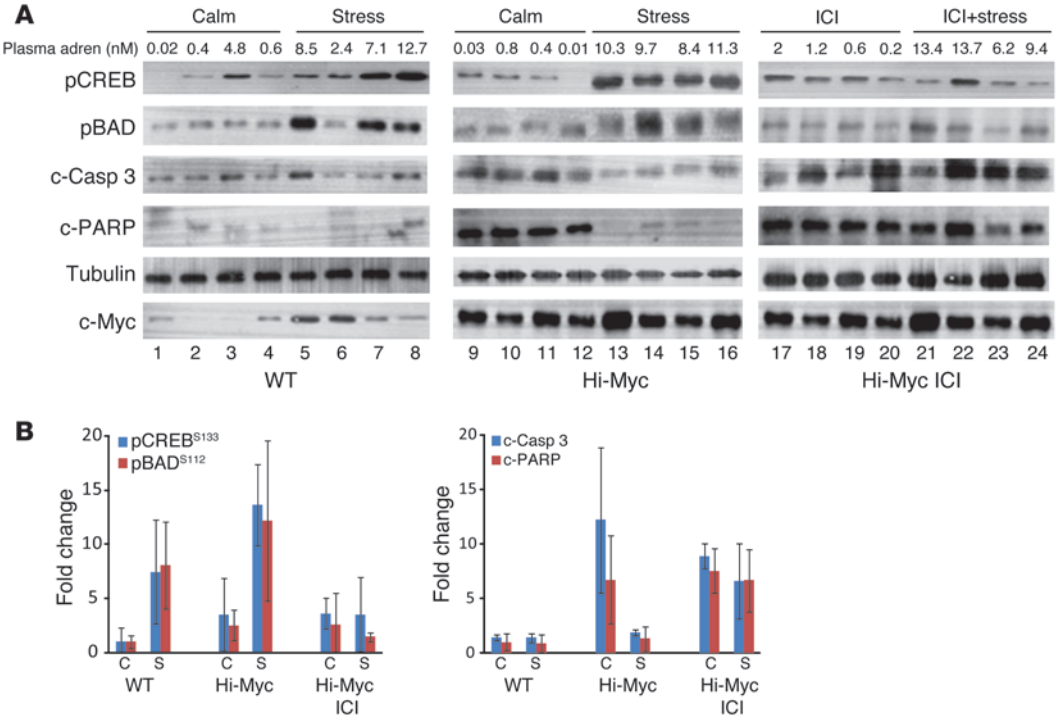

Figure 4

Stress induces BAD phosphorylation and inhibits cleavage of PARP and caspase-3 in Hi-Myc mouse prostate glands. WT and Hi-Myc mice were subjected to recurrent 1-hour immobilization stress at 12-hour intervals for 7 consecutive days; blood and prostates were collected immediately after the last stress procedure. ICI118,551 was given 30 minutes before stress. (**A**) Western blot analysis of DLP glands excised from intact (denoted "calm" or "C") and stressed ("stress" or "S") mice was conducted with antibodies to pCREB^{S133}, pBAD^{S112}, cleaved caspase-3, cleaved PARP, α-tubulin, and c-Myc. 4 representative samples from each treatment group are shown. (**B**) Densitometric analysis of Western blots revealed statistically significant increases of BAD and CREB phosphorylation in stressed versus intact mice (pBAD^{S112}, $P = 0.005$ between WT groups; $P = 0.02$ between Hi-Myc groups; pCREB^{S133}, $P = 0.02$ between WT groups; $P = 0.0019$ between Hi-Myc groups) and reduced cleavage of caspase-3 ($P = 0.005$) and PARP ($P = 0.01$) in stressed versus intact Hi-Myc mice. These effects of stress were completely eliminated by ICI118,551. Each experimental group contained at least 5 mice. Error bars represent SD from the average of at least 5 samples.

types, including prostate epithelial cells (29, 30); however, it did not increase BAD phosphorylation (Figure 4A). At the same time, subjecting mice to immobilization stress increased BAD phosphorylation in prostates of WT and Hi-Myc mice and decreased cleavage of caspase-3 and PARP in Hi-Myc prostates (Figure 4, A and B). Furthermore, immobilization stress administered for 7 consecutive days led to increased prostate weight in Hi-Myc mice, but not WT mice (Figure 5A). Histological analysis of prostate tissue sections revealed reduced apoptosis, based on increased numbers of cells with active caspase-3 or with positive TUNEL staining (Figure 5B and Supplemental Figure 7), and larger PIN area (Figure 5C), in Hi-Myc mice subjected to stress. Consistent with our results in C42 xenografts, stress-induced phosphorylation of BAD, inhibition of apoptosis, more extensive PIN, and increased prostate weight were all blocked in stressed mice by the ADRB2 antagonist ICI118,551 (Figures 4 and 5).

Tumor-promoting effects of behavioral stress depend on BAD phosphorylation. To test whether BAD phosphorylation is necessary for the effects of stress on prostate tumors, we used mice with BAD^{3SA} knockin and c-Myc expression (referred to herein as Hi-MycBAD$^{3SA/WT}$ mice). BAD$^{3SA/3SA}$ knockin mice are generated by replacing endogenous BAD with mutant BAD in which the major phosphorylation sites S112, S136, and S155 are substituted by alanines (14). Because homozygous knockin Hi-MycBAD$^{3SA/3SA}$ mice were born at lower than expected frequency and often had smaller body weights and smaller prostates, we decided to use heterozygous knockin Hi-MycBAD$^{3SA/WT}$ mice and WTBAD$^{3SA/WT}$ littermates that showed similar phenotypes.

Analysis of BAD phosphorylation and of apoptosis markers (cleaved PARP and cleaved caspase-3) revealed no difference between prostates from intact or stressed Hi-MycBAD$^{3SA/WT}$ mice; however, pCREB^{S1133} in prostates of stressed mice was significantly increased (Figure 6, A and B, and Supplemental Figure 8, A and B), which confirmed that stress activated the PKA pathway. Analysis of prostate tissue sections showed that, similar to WTBAD$^{3SA/WT}$ littermates, Hi-MycBAD$^{3SA/WT}$ mice were characterized by PIN, predominantly in the dorsolateral prostate (DLP) lobe. At the same time, there were no significant differences in prostate weight between Hi-MycBAD$^{3SA/WT}$ mice subjected to repeated immobilization stress or left intact (Figure 6, C and D), in striking contrast to Hi-MycBAD$^{WT/WT}$ mice, which express WT BAD (Figure 5A). Comparable results were obtained in 12- and 24-week-old Hi-MycBAD$^{3SA/WT}$ mice (Figure 6 and Supplemental Figure 8). Thus, similar to the C42 prostate cancer xenograft model, BAD phosphorylation was necessary for behavioral stress to manifest tumor-promoting effects in mouse prostate glands.

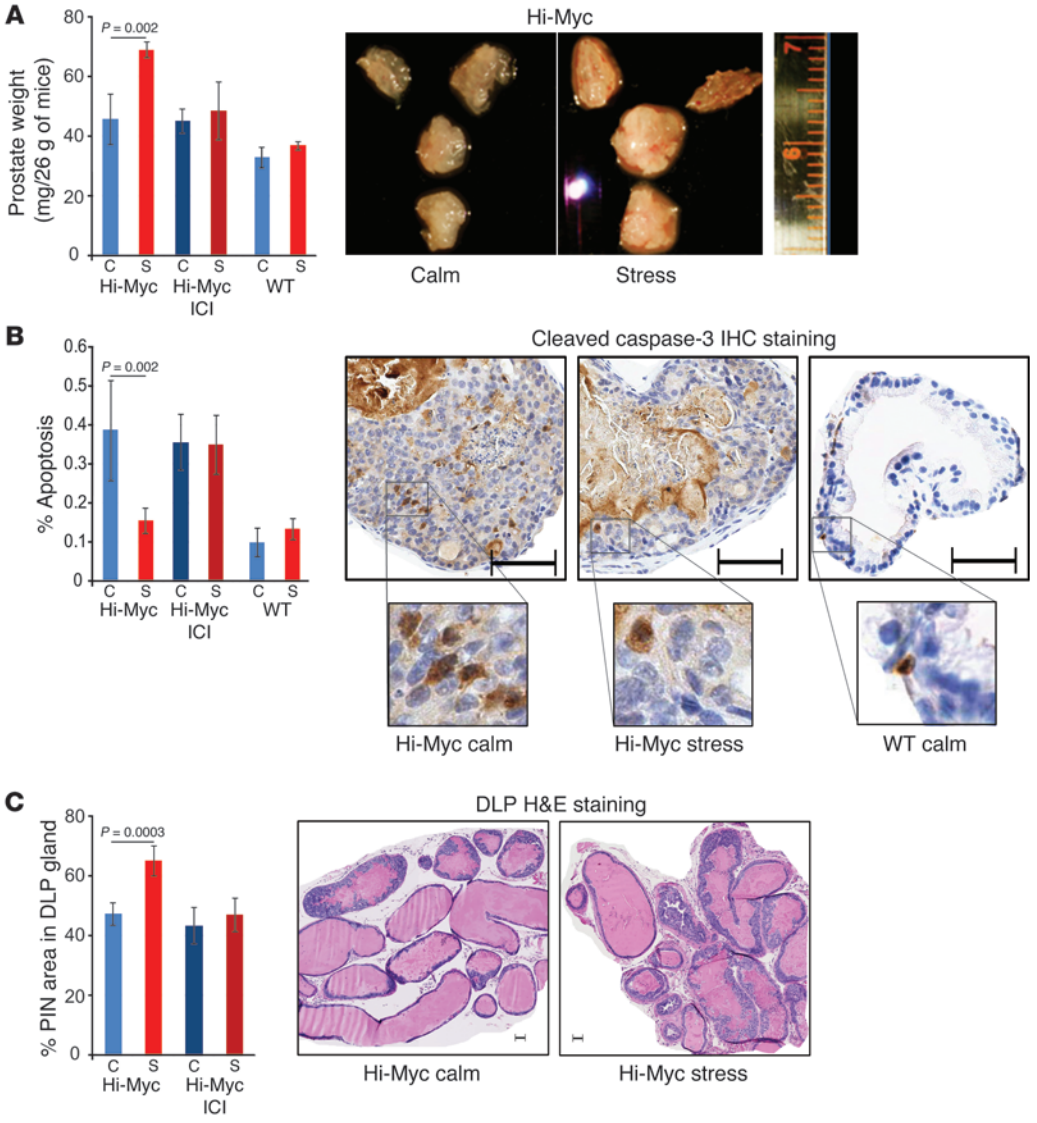

Figure 5

Stress accelerates PIN growth and inhibits apoptosis in DLP glands of Hi-Myc mice. (**A**) Stress increased prostate weight. Mouse prostates (AP, DLP, and VP lobes) were dissected and weighed, and the total prostate wet weight was expressed as mg/25 g body weight. Statistically significant differences were observed between intact and stressed Hi-Myc mice (P = 0.002), but not between WT groups (P = 1.00). This difference in Hi-Myc mice was eliminated by ICI118,551 injection prior to stress (P = 0.49). (**B**) Stress reduced apoptosis in DLP glands. Percent cleaved caspase-3–labeled cells in immunostained sections was determined relative to the total number of glandular epithelial cells in whole sections of DLP. Representative images of cleaved caspase-3 IHC-stained sections from DLP of intact or stressed Hi-Myc mice are also shown. Scale bars: 50 μm. Insets show the original images (×40 objective) enlarged ×5. (**C**) Stress increased PIN in DLP glands of Hi-Myc mice. Percent PIN area was determined as area of PIN divided by total DLP glandular area. Representative microphotographs of H&E-stained sections from DLP glands of intact and stressed Hi-Myc mice are also shown. Scale bars: 50 μm. See Supplemental Figure 8D for morphology of mouse PIN. Error bars in **A**–**C** show SD from the average of at least 5 samples.

Behavioral stress delays bicalutamide-induced involution and apoptosis in prostates of Hi-Myc mice. Androgen ablation therapy, introduced by Huggins in 1941, remains the most effective systemic treatment for prostate cancer (reviewed in ref. 31). Bicalutamide, an androgen receptor (AR) antagonist that, upon binding, inhibits transcriptional activity of AR, is widely used to treat prostate cancer. Since AR activity is necessary for survival of prostate cells, bicalutamide induces apoptosis and involution of human and rodent prostates (32–34).

We examined effects of systemically injected bicalutamide on prostates of Hi-Myc mice. The most significant reduction in prostate weight (from 45 ± 8.3 mg to 29 ± 8.4 mg) was observed after 2 daily injections of bicalutamide, with little further decrease (to 28 ± 3.7 mg) after third bicalutamide injection. Effects of behavioral stress on prostate weight were also most evident after 2 days of bicalutamide injections; therefore, this time point was selected for subsequent experiments. As shown in Figure 7, behavioral stress delayed Hi-Myc prostate involution and apoptosis induced by bicalutamide and increased prostate weight in bicalutamide-treated stressed versus intact Hi-Myc mice. Consistent with the effects on prostate weight, stress caused a significant 3.6-fold reduction in apoptosis, based on the percentage of cells with cleaved caspase-3 (Figure 7B). Analysis of Hi-Myc prostates by Western blotting confirmed quantitative analysis of apoptosis: cleaved caspase-3 and cleaved PARP were increased in prostates of mice that received bicalutamide (Figure 8A). Behavioral stress induced pCREB^{S133} and pBAD^{S112} and inhibited apoptosis, as shown by lower levels of cleaved caspase-3 and cleaved PARP, in prostates of stressed mice (Figure 8, B and C). Expression of probasin, a known androgen-responsive gene, was significantly reduced in prostates of bicalutamide-treated mice, yet no significant increase in probasin expression was detected in stressed mice (Figure 8, A and D), which indicates that stress does not transactivate AR signaling or activate transcriptional targets of AR.

The effect of stress on prostate weight was completely blocked by the ADRB2 antagonist ICI118,551 and was decreased from 2-fold

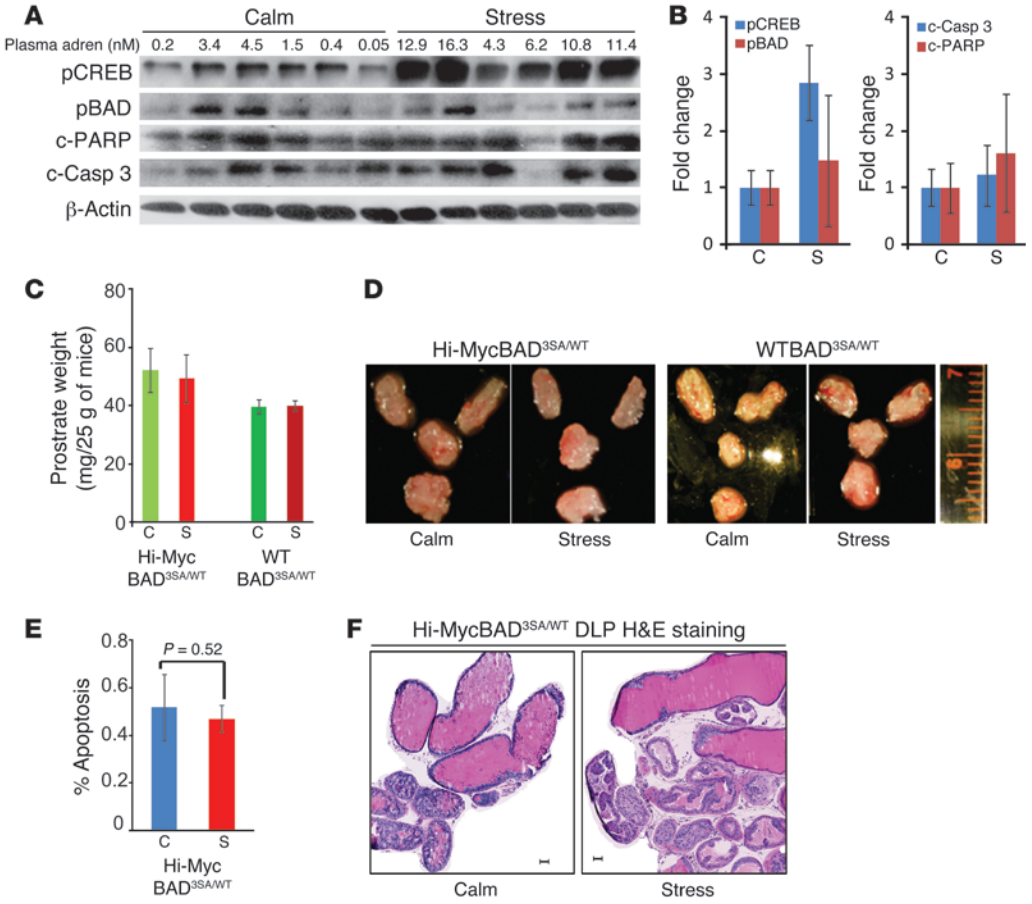

Figure 6

Antiapoptotic and tumor-promoting effects of stress are eliminated in BAD$^{3SA/WT}$ knockin mice. (**A**) Western blot analysis of DLP glands excised from 12-week-old intact and stressed Hi-MycBAD$^{3SA/WT}$ mice was conducted with antibodies to pCREB^{S133}, pBAD^{S112}, cleaved caspase-3, cleaved PARP, and β-actin. (**B**) Densitometric analysis of Western blots revealed statistically significant increases of pCREB^{S133} in stressed versus intact Hi-MycBAD$^{3SA/WT}$ mice ($P = 0.003$); however, no significant differences between intact and stressed mice were found in pBAD^{S112} ($P = 0.29$), cleaved caspase-3 ($P = 0.47$), or cleaved PARP ($P = 0.25$). Lysates of 4 intact mice were used for densitometry (2 mice with adrenalin levels greater than 1 nM were excluded as erroneously stressed); the stressed group contained 6 mice. (**C**) Prostates of intact and stressed Hi-MycBAD$^{3SA/WT}$ ($n = 5$ per group) and WTBAD$^{3SA/WT}$ ($n = 3$ per group) mice were analyzed as in Figure 3B. (**D**) Microphotographs of dissected prostate glands from Hi-MycBAD$^{3SA/WT}$ or WTBAD$^{3SA/WT}$ mice either subjected to repeated immobilization stress for 7 days or left intact. (**E**) Prostates of intact and stressed Hi-MycBAD$^{3SA/WT}$ mice were analyzed as in Figure 5B ($n = 5$ per group). Bars in **B**, **C**, and **E** show SD. (**F**) Representative images of H&E-stained sections of DLP glands of intact or stressed Hi-MycBAD$^{3SA/WT}$ mice. Scale bars: 50 μm.

Discussion

The experiments presented above demonstrated that in 2 distinct in vivo models of prostate cancer, C42 xenografts and prostates of Hi-Myc mice, behavioral stress activated the adrenaline/ADRB2/PKA/BAD antiapoptotic signaling pathway, which in turn reduced therapeutic sensitivity and accelerated prostate cancer development. These data introduce behavioral stress as a new environmental component contributing to prostate cancer pathogenesis through a defined antiapoptotic signaling pathway that impinges on BAD phosphorylation. Considering that prostate cancer diagnosis increases stress and anxiety levels (6, 7), activation of a stress-induced antiapoptotic pathway may lead to a vicious cycle of stress and cancer progression (Figure 9).

Numerous publications have demonstrated that BAD phosphorylation is necessary for inhibition of apoptosis by survival agonists in tissue culture models, including prostate cancer cell lines (11, 22, 35). However, the in vivo evidence supporting the role of BAD phosphorylation is circumstantial, and therefore cannot distinguish whether BAD phosphorylation plays a dominant or secondary role in translating survival signaling into tumor progression and therapy resistance. The results presented here are the first to establish the critical role of BAD phosphorylation in stress or adrenaline antiapoptotic signaling in prostate tumors in vivo.

In the context of prostate cancer, substantial attention is paid to the potential roles of ARs in regulation of apoptosis in prostate cells. Specifically, androgen independence is attributed to transactivation of AR in the absence of androgens by other signaling pathways or to activation of antiapoptotic and proliferative pathways that are entirely independent from AR (36). Several publications examined interactions between PKA signaling and AR and reported either transactivation (37, 38) or inhibition (39, 40) of AR.

We previously demonstrated that the antiapoptotic effect of activation of ADRB2s is modestly diminished in prostate cancer cells with knockdown of AR expression and thus is largely independent

to 0.2-fold in Hi-MycBAD$^{3SA/WT}$ prostates (Figure 7). Conversely, no significant decrease of apoptosis was observed in prostates of Hi-MycBAD$^{3SA/WT}$ mice or of mice that received ICI118,551 (Figure 7). Western blot analysis showed that BAD phosphorylation was completely blocked in mice that received ICI118,551 as well as in compound transgenic Hi-MycBAD$^{3SA/WT}$ mice (Figure 8, A and B). Consistent with lack of BAD phosphorylation, stress did not significantly decrease cleaved PARP and cleaved caspase-3 in prostates of Hi-MycBAD$^{3SA/WT}$ mice or mice treated with ICI118,551 (Figure 8, A and C). Taken together, results from experiments with Hi-Myc mice support our conclusion drawn from the xenograft experiments: antiapoptotic signaling via the adrenaline/ADRB2/PKA/BAD pathway in prostate cells plays a decisive role in the effects of behavioral stress on prostate cancer.

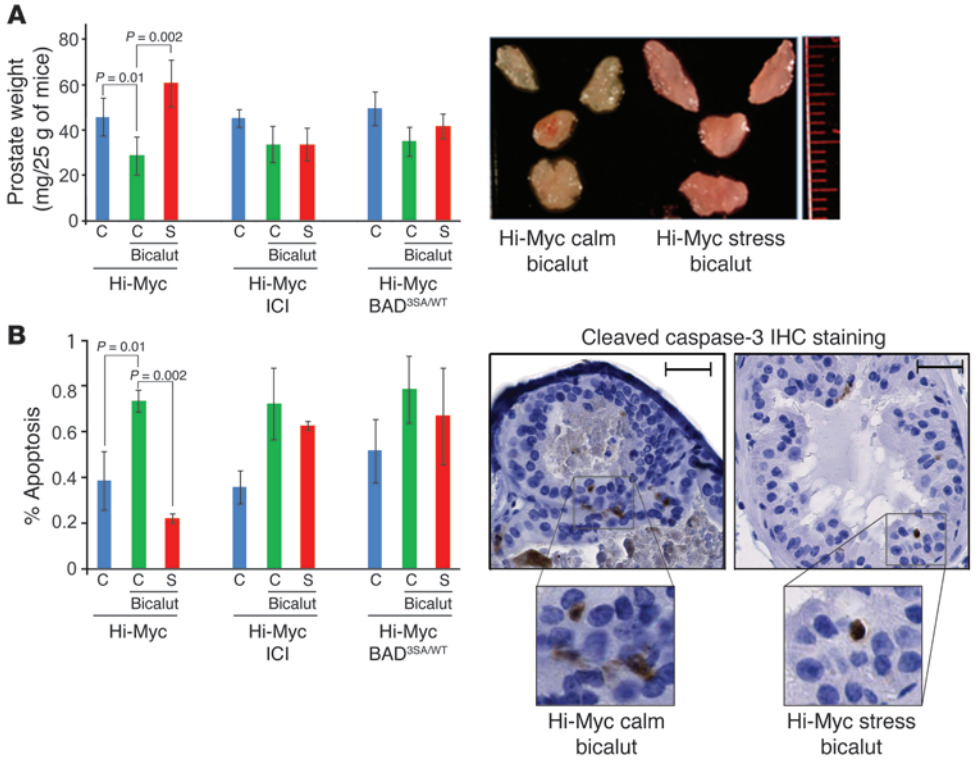

Figure 7

Stress delays bicalutamide-induced involution and apoptosis in Hi-Myc prostates via the ADRB2/BAD pathway. Hi-Myc mice were subjected to subcutaneous injection of bicalutamide (bicalut.; 50 mg/kg, once daily) and recurrent 1-hour immobilization stress at 12-hour intervals for 3 consecutive days; blood and prostates were collected immediately after the last stress procedure. ICI118,551 was given 30 minutes before stress. (**A**) Stress delayed bicalutamide-induced prostate involution in Hi-Myc mice. Mouse prostates (AP, DLP, and VP lobes) were dissected and weighed, and the total prostate wet weight was expressed as mg/25 g body weight. Statistically significant differences were observed between intact and bicalutamide-treated intact Hi-Myc mice ($P = 0.01$) and between bicalutamide-treated intact and stressed Hi-Myc mice ($P = 0.002$). The effect of bicalutamide on prostate weight was completely eliminated with ICI118,551 ($P = 0.54$) and significantly reduced from 2- to 0.2-fold in Hi-MycBAD$^{3SA/WT}$ mice ($P = 0.049$). Representative images of prostates of Hi-Myc intact and stressed mice treated with bicalutamide are also shown. (**B**) Stress delayed bicalutamide-induced apoptosis in DLP glands of Hi-Myc mice ($P = 0.002$). The effect of stress on bicalutamide-induced apoptosis was eliminated in Hi-Myc mice injected with ICI118,551 ($P = 0.84$) and in compound transgenic Hi-MycBAD$^{3SA/WT}$ mice ($P = 0.47$). Representative images of cleaved caspase-3 IHC-stained sections from DLP of intact and stressed Hi-Myc mice treated with bicalutamide are also shown. Scale bars: 50 μm. Insets show the original images (×40 objective) enlarged ×2.33.

from AR (11). Conversely, unlike the AR agonist R1881, adrenaline did not induce increased PSA production by LNCaP and C42 cells that express AR (Supplemental Figure 9A). Thus, adrenaline cannot transactivate AR in prostate cancer cells. Consistent with this conclusion, stress did not increase PSA levels in mice with C42Luc xenografts (Supplemental Figure 9B), or probasin expression in prostates of mice treated with bicalutamide (Figure 8A).

Considering these recent data and earlier results of experiments with AR knockdown, we concluded that transactivation of AR plays a limited role in the antiapoptotic effects of adrenaline. Instead, adrenaline bypasses AR by activating the AR-independent ADRB2/PKA/BAD antiapoptotic signaling pathway and thus increases resistance of prostate cancer cells to androgen ablation therapy and other cytotoxic therapies that induce apoptosis.

A substantial body of literature describes the effects of stress on tumor development and metastases in various cancer models (5). Yet despite this abundant phenomenology, mechanisms of interaction between stress and cancer have not been well defined. The pioneering studies by Selye on stress-induced immunosuppression (41) stimulated significant interest in understanding how the modulation of immune responses by stress contributes to cancer initiation and progression. Thus, it was reported that catecholamine signaling accelerated primary tumor development by inhibiting natural killer cells and stimulated metastatic spread by attracting macrophages to tumor sites (42, 43).

Another line of research has focused on stress-regulated angiogenesis. Experiments in ovarian tumor xenografts have shown that ADRB2 activation leads to greater production of VEGF by ovarian cancer cells and neovascularization that supports tumor growth (16). These experiments established a new paradigm that connected the neuroendocrine system, cancer cells, and vascular growth into a stress-activated circuit that accelerated progression of ovarian cancer (44).

Since our xenograft experiments were conducted in immunocompromised mice, and the effects of stress on apoptosis were observed within 6 hours, contributions from the tumor microenvironment are unlikely to play a dominant role in inhibiting apoptosis in this model. Moreover, we did not find increased VEGF levels in plasma of stressed mice (Supplemental Figure 10A). Because C42Luc xenografts are already highly vascularized, this model may not permit detection of vascularity increases. Immunostaining of the prostates of intact and stressed Hi-Myc mice with the endothelial cell marker factor VIII–related antigen (FVIII-RA) did not show increased vascular density in stressed mice (Supplemental Figure 10B). Taken together, these experimental data suggest that, unlike in the models of ovarian cancer, increased vascularity is not a primary mediator of stress effects on prostate tumors.

Expression of functional ADRB2 was previously reported in normal prostate epithelium and in prostate cancer cells, including LNCaP and C42 human prostate cancer cells and rodent prostates (12, 20, 45, 46). We confirmed expression of ADRB2 in prostate cancer models (Hi-Myc mouse prostates and C42 prostate cancer cells) as well as in human prostates (Supplemental Figure 11). Our results showing inhibition of antiapoptotic effects of

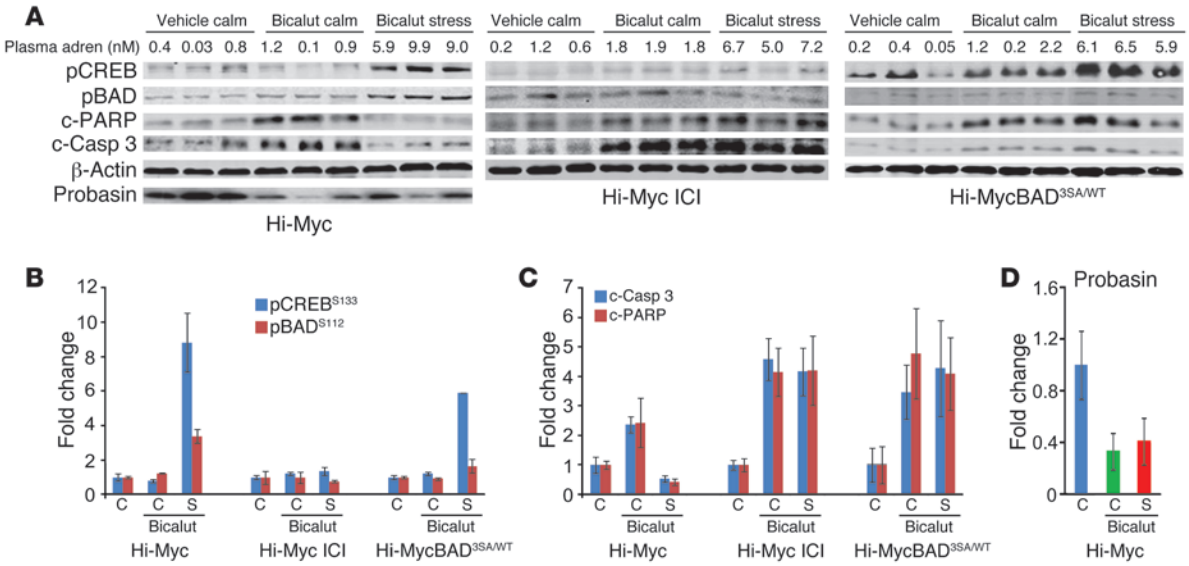

Figure 8

Stress inhibits bicalutamide-induced cleavage of PARP and caspase-3 through ADRB2 and BAD phosphorylation in prostates of Hi-Myc mice. (**A**) Western blot analysis of prostate glands excised from intact mice and bicalutamide-injected intact or stressed mice was conducted with antibodies to pCREB^{S133}, pBAD^{S112}, cleaved caspase-3, cleaved PARP, β-actin, and probasin. 3 representative samples for each treatment group are shown. (**B**) Densitometric analysis of Western blots showed significant increases of BAD and CREB phosphorylation in stressed versus intact Hi-Myc mice (pCREB^{S133}, $P = 0.01$; pBAD^{S112}, $P = 0.008$), which was blocked by ICI118,551. No significant differences were found in pCREB^{S133} ($P = 0.35$) or pBAD^{S112} ($P = 0.34$) between the intact and stressed bicalutamide treatment groups. In Hi-MycBAD$^{3SA/WT}$ mice, stress significantly increased pCREB^{S133} ($P = 0.003$), but not pBAD^{S112} ($P = 0.15$). (**C**) Stress decreased cleavage of caspase-3 and PARP induced by bicalutamide ($P = 0.003$, intact vs. bicalutamide intact; $P = 0.004$, bicalutamide intact vs. bicalutamide stress). These effects were eliminated in mice treated with ICI118,551 and in Hi-MycBAD$^{3SA/WT}$ mice ($P > 0.5$). *P* values were similar for cleaved caspase-3 and PARP. (**D**) Bicalutamide treatment significantly decreased probasin expression ($P = 0.01$), and stress did not affect probasin expression in prostates of bicalutamide-treated mice ($P = 0.58$). Each experimental group contained at least 5 mice. Error bars in **B**–**D** show SD from the average of at least 4 samples.

stress or adrenaline in C42Luc xenografts by inducible expression of PKI-GFP and of BAD^{S112A} in prostate cancer cells are consistent with the notion that activation of antiapoptotic signaling within prostate cancer cells (rather than systemic effects of adrenaline) are responsible for reduced therapeutic sensitivity and accelerated progression of prostate tumors. Results from experiments in Hi-Myc mice that express either WT BAD or BAD^{3SA} supported the conclusions from experiments in the xenograft model that antiapoptotic signaling via BAD phosphorylation mediates effects of stress on PIN extent and on prostate weight. These results suggest apoptosis inhibition by adrenaline as a new mechanism of the tumor-host interaction that, together with effects mediated via the immune and vascular systems, defines the effects of behavioral stress on tumor growth.

Interactions between stress and cancer may not always be unidirectional. Thus, moderate stress from enriched environments reportedly causes inhibition of tumor growth and cancer remission in melanoma and colon cancer models (47). These antitumor effects of moderate stress are attributed to increased hypothalamic brain-derived neurotrophic factor that activates sympathetic β-adrenergic receptor signaling, which in turn reduces secretion of leptins by white adipose tissue (47). Unlike immobilization stress, enriched environments may not increase blood adrenaline sufficiently to activate antiapoptotic signaling in cancer cells. These bidirectional effects of behavioral stress evoke the distinction between "eustress" and "distress" made by Selye in his classic studies (41).

Several extrapolations relevant to human prostate cancer can be derived from our results. First, tumor-promoting effects of stress will be evident in patients who regularly experience increased adrenaline levels. We observed repeated increases greater than 1 nM in plasma adrenaline levels of 14 of 62 prostate cancer patients (22%; Supplemental Figure 12).

Second, antiapoptotic effects of stress will be restricted to cancer cells that express components of the ADRB2/PKA/BAD pathway. ADRB2, PKA, and BAD are ubiquitously expressed in normal prostate epithelial cells and in prostate cancer cells (20, 45, 48–50). Expression of ADRB2 is regulated by androgen and triiodothyronine and is reportedly increased in malignant prostate glands and in metastatic tumors (45). Yet another publication showed biphasic changes in ADRB2 expression characterized by increased levels of PIN and localized prostate cancer, followed by reduction of ADRB2 in metastatic cancer specimens due to transcriptional suppression by EZH2 (51). Still, despite apparent EZH2-dependent downregulation of ADRB2 in LNCaP cells, adrenaline in concentrations observed in stressed patients can protect these cells from apoptosis (11). There is also evidence that expression of βARK1, which desensitizes ADRB2, is lost in prostate tumors with high Gleason scores. This may lead to prolonged activation of adrenaline/ADRB2/PKA/BAD signaling (52).

Third, effects of behavioral stress would be most evident when apoptosis plays the leading role: for example, in tumors with deregulated oncogene expression. We have shown accelerated tumor progression in Hi-Myc mice subjected to repeated stress. Considering that increased c-MYC expression is reported in a sub-

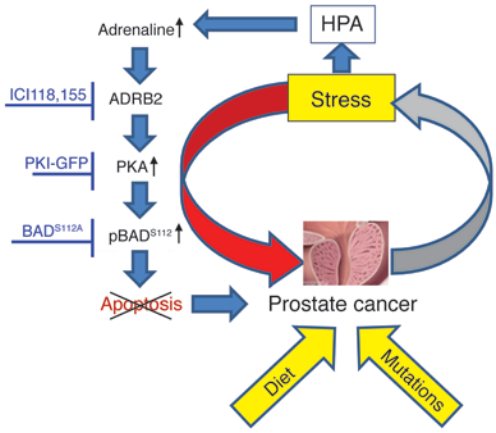

Figure 9
A vicious circle of stress signaling in prostate cancer. Psychoemotional stress activates the hypothalamic-pituitary-adrenal axis (HPA); as a result, blood levels of adrenaline increase and activate ADRB2/PKA/BAD antiapoptotic signaling in prostate cells. Constitutive activation of this signaling pathway in stressed patients (Supplemental Figure 12) may trigger a vicious circle: stress and anxiety from a diagnosis of prostate cancer increase adrenaline levels that in turn reduce efficacy of anticancer treatments.

stantial proportion of prostate cancers (53), stress-induced apoptosis suppression could synergize with c-MYC in prostate cancer development in men.

Fourth, considering the redundancy of the signaling pathways that control apoptosis, effects of stress in a given tumor will depend on activity of other pathways. For example, if the Ras/ERK or PI3K pathways that control phosphorylation of BAD^{S112} (corresponding to human BAD^{S75}) are active, then stress signaling may have a lesser effect. Thus, in advanced prostate cancers that have lost PTEN, stress is not expected to have a significant effect unless patients are treated with PI3K inhibitors.

We are at the very beginning of understanding complex stress-cancer interactions, with multifaceted responses to stress that affect cancer cells, tumor microenvironment, and the organism overall. There is a vast body of literature on psychological disorders experienced by cancer patients (54), and yet very little is known about the changes in the "endocrinome" of cancer patients caused by behavioral stress. In addition, the limited mechanistic information on signaling by stress hormones in various tumor cells makes it difficult to design new epidemiological studies and to interpret the results of previous ones that have addressed the role of stress in cancer progression and the therapeutic potential of beta blockers as an adjuvant anticancer therapy. Together with recent reports on stress-induced VEGF and IL-8 secretion (16, 55), activation of FAK (56), and downregulation of p53 (57, 58) that stimulate tumor angiogenesis, migration, invasion, and survival (26), our data highlight the connection between activation of the ADRB2/PKA axis and tumor-promoting effects of stress and introduce BAD phosphorylation as a target of stress or adrenaline signaling. Future experiments will determine whether stress activates the adrenaline/ADRB2/PKA/BAD pathway in prostate tumors and other human cancers. We anticipate that components of this signaling pathway could be used as biomarkers to predict whether and how a given tumor will respond to stress and antistress therapies.

Methods

Cell lines, antibodies, and reagents. C42LucBAD cells were generated by transfecting C42 cells with WT BAD (HA-BAD-pTRE2hygro) and firefly luciferase (PGL4.13). C42LucPKI cells were developed by cotransfecting C42tet-on cells with PKI-GFP chimera (PKI-GFP-pTRE-tight) and firefly luciferase (PGL4.14 hygro). C42LucBAD^{1SA} cells were developed by cotransfecting C42tet-on cells with mutant BAD^{1SA} (59) (HA-BAD^{1SA}-pTRE-tight), which has a mutated phosphorylation site at S112, and with firefly luciferase (PGL4.14 hygro). Transfections were performed at 60%–70% confluence using Lipofectamine 2000 (Invitrogen) according to the manufacturer's recommendations. All cell lines were maintained in RPMI 1640 with 10% fetal bovine serum in 5% CO_2 at 37°C. Selections of stable clones were carried out in the presence of G418 (600 μg/ml) and hygromycin (150 μg/ml). After a 3-week selection period, macroscopically visible colonies were picked based on luminescence (luciferase expression). Cells were then expanded and analyzed for doxycycline-inducible expression of HA-BAD, PKI-GFP, and HA-BAD^{1SA}. A2870 ovarian cancer cells, which do not express ADRB2, were provided by A. Sood (University of Texas MD Anderson Cancer Center, Houston, Texas, USA).

Antibodies were obtained from the following sources: BAD, pBAD^{S112}, pAKT^{308}, pAKT^{S473}, pCREB^{S133}, and cleaved caspase-3 from Cell Signaling Technology; mouse monoclonal antibody to β-actin from Sigma-Aldrich; goat polyclonal antibody to cleaved PARP from R&D Systems; anti-ADRB2 antibody from Olomone Labs; mouse monoclonal antibody to c-Myc (9E10) and goat polyclonal antibody to probasin (R-15) from Santa Cruz Biotechnology; rabbit polyclonal antibody to FVIII-RA (catalog no. 18-0018) from Zymed; and secondary horseradish peroxidase–conjugated antibodies used for Western blots from Amersham Biosciences. Protein G–agarose beads and adrenaline were obtained from Calbiochem. ZSTK474 was provided by Zenyaku-Kogyo Co. Ltd. G418 and hygromycin B were from Clontech. Bicalutamide (Casodex) was bought from Santa Cruz Biotechnology. All other chemicals and reagents, unless otherwise specified, were purchased from Sigma-Aldrich. Tissue culture reagents were purchased from Invitrogen.

Mouse xenograft model and acute stress. 6-week-old male athymic nude mice (BALB/c genetic background) were obtained from the National Cancer Institute. Mice were maintained under pathogen-free conditions and provided with sterile food and water ad libitum. Human tumor xenografts were generated by subcutaneously inoculating prostate cancer cell lines (C42LucBAD, C42LucPKI, and C42LucBAD^{1SA}) into nude mice. Each mouse received 4 subcutaneous injections of 2×10^6 cells with BD Matrigel matrix High Concentration (BD Biosciences). Injections were made using an insulin syringe and a 27-gauge needle at 4 locations: left and right shoulder and left and right flank. Injections at 4 locations ensured that each mouse would develop xenograft tumors, thus reducing the number of mice required for the experiments. When the largest tumor was approximately 100 mm^3 in size, HA-BAD, PKI-GFP, or BAD^{1SA} expression was induced by addition of doxycycline (1 mg/ml) to the drinking water 24 hours before the experiments. Mice were randomly assigned to experimental groups (DSMO; ZSTK474; ZSTK474 followed by immobilization stress; ZSTK474 and epinephrine; ZSTK474 and ICI118,551, followed by immobilization stress; and ZSTK474, ICI118,551, and epinephrine). The next day, xenograft tumors (1 tumor per mouse) were injected once with the PI3K inhibitor ZSTK474 (5 mM, 40 μl; 0.8 mg/kg) or vehicle (DMSO); 3 hours later, mice were subjected to immobilization stress for 1 hour (acute stress) or injected with adrenaline (100 μM, 30 μl). Immobilization stress, which mimicked the presence of a natural predator without possibility of escape, was created by placing mice into a 50-ml conical vial with openings for breathing. Vials with mice were placed for 1 hour in a plastic box that contained tissue impregnated with fox urine (Chagnon's Trap-

ping Supply). The ADRB2 antagonist ICI118,551 (25 μM, 30 μl) was given intraperitoneally 30 minutes before immobilization stress or adrenaline injection. To avoid unintended stress, mice were handled with extra care. Manipulations that could cause distress (e.g., injections and blood sampling) were conducted under light isoflurane anesthesia.

Xenograft tumors were monitored by noninvasive optical imaging on an IVIS100 imaging station (Caliper Life Sciences). Animals were immobilized by gas anesthesia with 2% isoflurane/O_2. To account for background and nonspecific luminescence, mice were imaged before injection of luciferin. Animals were injected with 100 μl of the firefly luciferase substrate luciferin (3.5 mg/ml in PBS) and imaged 15 minutes later. Whole-body images were obtained and analyzed using the Living ImageH software provided with the imaging system. A grayscale photographic image and the bioluminescent color image were superimposed to provide anatomic registration of the light signal. A region of interest (ROI) was manually selected over the luminescent signal, and the intensity was recorded as photons/second within an ROI. Luminescence was measured before injection of PI3K inhibitors (0 hours) and 24, 48, and 72 hours after injection. Xenograft tumors were excised 6 hours after injection of ZSTK474 and analyzed by immunohistochemistry for expression of cleaved caspase-3 and by Western blotting for expression of BAD, PKI-GFP, and BAD^{1SA}; inhibition of pAKT; cleavage of PARP and caspase-3; and phosphorylation of CREB and BAD. At the time of tumor excision, blood was also collected, and adrenaline levels were measured by ELISA (see below).

Mouse prostate model and chronic stress. The transgenic Hi-Myc mice used herein, in which the prostate-specific expression of human c-myc is driven by the rat probasin promoter with androgen-responsive elements (ARR2/probasin promoter; ref. 29), were obtained from the Mouse Repository of the National Cancer Institute Mouse Models of Human Cancer Consortium. Hemizygous Hi-Myc mice on FVB background were cross-bred with nontransgenic FVB breeders. All control mice used at each time point were from FVB littermates. To test the role of BAD phosphorylation, Hi-Myc mice were bred with $BAD^{3SA/3SA}$ knockin mice (provided by M. Greenberg, Harvard Medical School, Boston, Massachusetts, USA), in which endogenous BAD is replaced by mutant BAD with S112, S136, and S155 substituted for alanines (14). In these experiments, the second generation of Hi-$MycBAD^{3SA/WT}$ mice was compared with $WTBAD^{3SA/WT}$ littermates as controls for baseline measures of prostate weight and with Hi-$MycBAD^{WT/WT}$ littermates as controls for stress-induced reduction of apoptosis and increase in prostate weight.

12-week-old mice were subjected to immobilization stress for 1 hour for 7 consecutive days (2 times per day with 12-hour interval). To investigate the role of ADRB2 in stress effects, ICI118,551 (25 μM, 30 μl) was given intraperitoneally 30 minutes before immobilization stress. At the end of day 7, before sacrifice of animals, approximately 500 μl of blood per mouse was collected through heart puncture under deep isoflurane anesthesia; blood was stored at –80°C until analysis. After sacrifice, each mouse was weighed. Anterior prostate (AP), DLP, and ventral prostate (VP) lobes were dissected and weighed; prostate tissues were then paraffin embedded and snap frozen in liquid nitrogen.

In vivo bicalutamide injection in mouse stress model. 12-week-old mice were subjected to subcutaneous injections with either vehicle (DMSO) or bicalutamide (50 mg/kg) once a day and to immobilization stress for 1 hour (2 times per day with 12-hour interval) for 2 or 3 consecutive days. To investigate the role of ADRB2 in stress effects, ICI118,551 was given as described above. At 24 hours after the last injection, blood and prostate tissues (AP, DLP, and VP) were collected and processed as described earlier.

Blood collection from prostate cancer patients. Blood was collected by phlebotomy twice with a 4-week interval.

Adrenaline and noradrenaline measurements. Plasma adrenaline concentrations were measured by ELISA (mouse) or radioimmunoassay (mouse, human) using commercially available assays (BA-0100 and BA-5100; Labor Diagnostika Nord, purchased through Rocky Mountain Diagnostics). Adrenaline was first extracted using a cis-diol–specific affinity gel, acetylated to N-acyladrenaline, and then derivatized enzymatically to N-acylmetanephrine. Acylated adrenaline from the standards, controls, and samples then competed for a fixed number of antiserum binding sites, later detected by ELISA or radioimmunoassay, as described by the manufacturer.

For tissue adrenaline measurements, samples were homogenized in 0.01 N HCl in the presence of EDTA (final concentration, 1 mM) and sodium metabisulfite (final concentration, 4 mM), and adrenaline concentrations were measured by ELISA (mouse).

Tissue noradrenaline levels were quantified using HPLC (Agilent 1100 binary HPLC) tandem mass spectrometry (Waters Quattro Ultima). Frozen pulverized tissues were weighed, suspended in HPLC-grade methanol (Fisher Scientific), and homogenized by ultrasonic disruption using a Misonix 3000 tissue homogenizer. Samples were centrifuged at 15,000 *g* for 5 minutes at 5°C to pellet cellular debris, and 0.1 ml supernatant was then mixed 1:1 with 20 mM ammonium acetate (pH 3.5) for analysis. Chromatographic resolution of noradrenaline was achieved using a Phenomenex Synergi4 Hydro-RP (150 × 2 mm) analytical column with a linear mobile phase gradient separation method. Mass spectrometry analysis was performed using electrospray positive ionization in multiple reaction-monitoring modes.

VEGF ELISA. VEGF concentrations in the mouse plasma were measured using mouse VEGF Quantikine immunoassays (R&D Systems) following the manufacturer's instructions.

Immunoprecipitation. Prostate tissues were homogenized in lysis buffer containing 20 mM Tris (pH 7.4); 40 mM NaF; 2 mM EDTA; 1 mM EGTA; 1% Triton X-100; 1 mg/ml each of leupeptin, pepstatin, and aprotinin; 1 mM phenylmethylsulfonyl fluoride; 1 mM $NaVO_4$; 50 mM β-glycerophosphate; 40 mM *p*-nitrophenyl phosphate; and 1 mM dithiothreitol. The lysates were cleared of insoluble material by centrifugation at 18,400 *g* for 10 minutes at 4°C. Tissue extracts were incubated with 6–8 μg anti-HA antibodies (12CA5) overnight at 4°C and with protein G–agarose beads (Calbiochem) for another 3 hours. Beads were washed 3 times with cell lysis buffer, and proteins were eluted with SDS sample buffer for Western blot analysis.

Western blot analysis. Tissue or cell lysates with equal amounts of total protein were separated by PAGE and transferred to nitrocellulose membranes for analysis with appropriate antibodies. The membranes were incubated overnight at 4°C with primary antibodies against pCREB, pAKT, AKT, pBAD, BAD, cleaved caspase-3, and GFP (Cell Signaling Technology); β-actin; and c-Myc and cleaved PARP (Santa Cruz), followed by 1 hour of incubation at room temperature with secondary horseradish peroxidase–conjugated polyclonal anti-rabbit antibody from donkeys (1:5,000 dilution; Amersham), anti-mouse IgG, HRP-Linked Whole Ab from sheep (1:5,000 dilution; GE Healthcare NA931), or anti-goat IgG, HRP-Linked Whole Ab from cows. Proteins were visualized using an ECL chemiluminescence detection system, following the manufacturer's protocol and Hyperfilm ECL (Amersham). After staining, nitrocellulose blots were stripped and reprobed with loading control antibodies (β-actin, α-tubulin, AKT, and BAD) for comparison and normalization. For quantification of Western blots, fluorescent secondary antibodies were used, and signal was quantified on an Odyssey imaging system.

Immunohistochemistry. Antibody staining was performed on histological sections of formalin-fixed prostate tumor xenografts and mouse prostate lobes. Cleaved caspase-3 staining was performed with an anti–cleaved caspase-3 primary antibody (1:1,000 dilution; catalog 9661; Cell Signaling Technology) that specifically recognizes the large fragment (17 kDa) of the active protein but not full-length caspase-3, followed by a biotinylated anti-rabbit secondary antibody and streptavidin alkaline phosphatase (Super Sensitive Link-Label IHC Detection Systems; Bio-Genex); sections were then visual-

ized with Vector Red Substrate (SK-5100; Vector Laboratories) and counterstained with hematoxylin. Similarly, Ki-67 immunostaining was performed with polyclonal anti–Ki-67 (1:200 dilution; ab15580; Abcam) antibody.

Double immunofluorescence for cleaved caspase-3 and TUNEL. To visualize the colocalization of activated caspase-3 and DNA fragmentation in C42LucBAD prostate cancer cells, C42LucBAD prostate cancer xenografts, and mouse prostates, sequential immunofluorescence for cleaved caspase-3 and TUNEL was done as described previously (60). Briefly, cells and fresh-frozen tissue sections were fixed in 10% buffered formalin for 20 minutes and then permeabilized in 0.1% sodium citrate with 0.1% NP-40 at 4°C for 2 minutes, followed by blocking for 30 minutes with 2.5% goat serum in PBST (PBS plus 0.1% Tween 20) at 37°C. Primary antibody to cleaved caspase-3 (1:300 dilution in PBST with 2.5% goat serum; Cell Signaling Technology) was added for 3 hours at room temperature. After washing 3 times in PBST, secondary antibody conjugated with Texas Red (1:300 dilution in PBST plus 2.5% goat serum) was added for 90 minutes at room temperature. After washing 3 times in PBST, TUNEL reaction was done as described in the manual for In Situ Cell Death Detection Kit, POD (Hoffmann-La Roche Ltd.).

Determination of apoptotic and proliferative indices. For this study, activated cleaved caspase-3 labeling was used to identify apoptotic cells. The number of cleaved caspase-3–labeled cells in immunostained sections was counted relative to the total number of glandular epithelial cells present in whole DLP sections. Digital copies of the entire prostate were created automatically from the cleaved caspase-3–immunostained glass slides by the Aperio ScanScope CS with objective ×20. Individual images of DLP were then exported in Adobe Photoshop CS, and nonglandular portions of the DLP were cropped. The total number of DLP epithelial cells was enumerated in all glands using Image-Pro Plus 4.5 software (Image Processing Solutions). Numbers of apoptotic cells were then counted in every gland from the imaged DLP. The apoptotic index for each DLP lobe was expressed as the number of apoptotic cells per 100 cells in all glands (glands with normal epithelium and PIN). The Ki-67 proliferative index was determined similarly.

PIN measurements in Hi-Myc mice. Hi-Myc mice develop mouse PIN followed by prostatic adenocarcinoma as a result of MYC overexpression in the mouse prostate. Histologically, mouse PIN is characterized by enlargement of nuclei, prominence of nucleoli, and epithelial cell proliferation; crowding results in a pseudo-multilayer appearance (overlapping of cells), with normal architecture of the glands (Supplemental Figure 2E). PIN area was measured in DLP of intact and chronically stressed mice. H&E-stained slides were digitally scanned, exported, and cropped as described above. PIN and total glandular areas were measured in each scanned DLP, and PIN results were expressed as a percentage of total DLP glandular area.

In vivo MRI for tumor volume measurements. Each animal was anesthetized in an induction chamber filled with a mixture of isoflurane (2%) and oxygen (2 l/min) and continued to receive isoflurane and oxygen during the procedure; typical levels during scanning were 1.5% and 1 l/min. A respiration pillow was placed over the animal's abdomen to monitor respiration rate and to facilitate triggered acquisition. Thermostatically controlled warm air was blown into the bore of the magnet to keep the animal's skin temperature above 35°C. The animal was placed in the center of the 7T MRI magnet in a 50-mm-inside-diameter quadrature RF coil (Doty Scientific). Whole-body T2-weighted images were acquired using low 300.2-Mhz radio waves. The entire imaging data acquisition procedure took about 15 minutes per mouse. A 3-plane localizer Rapid Acquisition with Relaxation Enhancement (RARE) pulse sequence was used with the following parameters: TR, 2100 ms; TE, 36 ms; matrix, 256 × 256; FOV, 4 cm; slice thickness, 2.0 mm; NEX, 1; giving an acquisition time of 50 seconds. The 3-plane localizer was used to plan the geometry for the high-resolution tumor volume scan. The high-resolution scan was performed using a RARE pulse sequence as well as axial slices centered on the tumor, with the following parameters: TR, 3,300 ms; TE, 45 ms; FOV, 3.0 cm; slice thickness, 1.0 mm; matrix, 256 × 256; NEX, 2; giving an acquisition time of 10 minutes. At the end of the procedure, each mouse was placed on a warming pad until it regained consciousness. Images were analyzed using ImageJ software to measure the total tumor volume in each mouse.

Total PSA electrochemiluminescence immunoassay. Total PSA was assayed according to the manufacturer's protocol, using a Roche Elecsys 2010 Chemistry Analyzer (Hoffmann-La Roche Ltd.) (61). Each sample was assayed in triplicate.

Analysis of microvessel density (MVD) in mouse prostate tissue sections. FVIII-RA expression was detected immunohistochemically using rabbit polyclonal antibody (Zymed FVIII-RA antibody) provided by L. Metheny-Barlow (Wake Forest University School of Medicine) on histological sections of formalin-fixed mouse prostate lobes. To quantify MVD, we counted total number of microvessels (clusters of endothelial cells positive for FVIII staining with central lumen were considered to be individual vessels) from digital copies of the entire prostate. MVD was then expressed as number of microvessels per square millimeter of prostate tissue section.

Statistics. To compare luminescence between mouse groups in Figures 1 and 2, 2-way repeated-measures ANOVA models were fit with the individual animal treated as a random effect in the model. In these models, time and group were considered as fixed effects. For each model, the group by time interaction was first examined to determine whether differences between groups were consistent over the time periods. If this interaction was nonsignificant, then the model was refit without the interaction term, and the group effect was examined, adjusting for the time of the measurement. Groups were compared using this approach. PROC MIXE in SAS version 9.2 was used to fit these models.

To determine whether differences between data sets in Figure 3–8 and Supplemental Figures 6 and 8–10 were statistically significant, Student's *t* test analysis (2-tailed distribution; 2-sample unequal variance) was performed using Microsoft Excel software. A P value less than 0.03 was considered significant. Error bars show SD from the average of at least 3 samples.

Study approval. All animal studies were conducted according to a protocol approved by the Institutional Animal Care and Use Committee of Wake Forest School of Medicine and conformed to the NIH Guide for the Care and Use of Laboratory Animals. For studies in prostate cancer patients, all participants provided informed consent, and the protocol was approved by the Institutional Review Board of Wake Forest School of Medicine.

Acknowledgments

The authors are grateful to Anil Sood and Karen Klein for critical reading and helpful suggestions; to Dina Yamaleeva, Michael Mangiapani, and Michael Conlin for assistance with image analysis; to John Olson for MRI imaging; and to Michael Thomas for mass spectrometry detection of noradrenaline. This work was supported by federal grants PC073548 from the Department of Defense and R01CA118329 from the National Cancer Institute and by institutional grants from Wake Forest University Health Sciences to G. Kulik. D. Yancey was supported in part by Research Supplement to Promote Diversity in Health-Related Research.

Received for publication February 10, 2012, and accepted in revised form November 26, 2012.

Address correspondence to: George Kulik, Department of Cancer Biology, Wake Forest School of Medicine, Medical Center Blvd., Winston-Salem, North Carolina 27157, USA. Phone: 336.713.7650; Fax: 336.713.7661; E-mail: gkulik@wakehealth.edu.

1. Berkow SE, Barnard ND, Saxe GA, Ankerberg-Nobis T. Diet and survival after prostate cancer diagnosis. *Nutr Rev*. 2007;65(9):391–403.
2. Saxe GA, Major JM, Nguyen JY, Freeman KM, Downs TM, Salem CE. Potential attenuation of disease progression in recurrent prostate cancer with plant-based diet and stress reduction. *Integr Cancer Ther*. 2006;5(3):206–213.
3. Ornish D, et al. Changes in prostate gene expression in men undergoing an intensive nutrition and lifestyle intervention. *Proc Natl Acad Sci U S A*. 2008;105(24):8369–8374.
4. Spiegel D, Giese-Davis J. Depression and cancer: mechanisms and disease progression. *Biol Psychiatry*. 2003;54(3):269–282.
5. Armaiz-Pena GN, Lutgendorf SK, Cole SW, Sood AK. Neuroendocrine modulation of cancer progression. *Brain Behav Immun*. 2009;23(1):10–15.
6. Ullrich PM, Carson MR, Lutgendorf SK, Williams RD. Cancer fear and mood disturbance after radical prostatectomy: consequences of biochemical evidence of recurrence. *J Urol*. 2003;169(4):1449–1452.
7. Cohen L, et al. Cancer worry is associated with abnormal prostate-specific antigen levels in men participating in a community screening program. *Cancer Epidemiol Biomarkers Prev*. 2003;12(7):610–617.
8. Stone AA, Mezzacappa ES, Donatone BA, Gonder M. Psychosocial stress and social support are associated with prostate-specific antigen levels in men: results from a community screening program. *Health Psychol*. 1999;18(5):482–486.
9. Miller HC. Stress prostatitis. *Urology*. 1988; 32(6):507–510.
10. Perron L, Bairati I, Harel F, Meyer F. Antihypertensive drug use and the risk of prostate cancer (Canada). *Cancer Causes Control*. 2004;15(6):535–541.
11. Sastry KS, et al. Epinephrine protects cancer cells from apoptosis via activation of cAMP-dependent protein kinase and BAD phosphorylation. *J Biol Chem*. 2007;282(19):14094–14100.
12. Palm D, et al. The norepinephrine-driven metastasis development of PC-3 human prostate cancer cells in BALB/c nude mice is inhibited by beta-blockers. *Int J Cancer*. 2006;118(11):2744–2749.
13. Yemelyanov A, et al. Tumor suppressor activity of glucocorticoid receptor in the prostate. *Oncogene*. 2007;26(13):1885–1896.
14. Datta SR, et al. Survival factor-mediated BAD phosphorylation raises the mitochondrial threshold for apoptosis. *Dev Cell*. 2002;3(5):631–643.
15. Parker J, et al. Chronic stress accelerates ultraviolet-induced cutaneous carcinogenesis. *J Am Acad Dermatol*. 2004;51(6):919–922.
16. Thaker PH, et al. Chronic stress promotes tumor growth and angiogenesis in a mouse model of ovarian carcinoma. *Nat Med*. 2006;12(8):939–944.
17. Thalmann GN, et al. LNCaP progression model of human prostate cancer: androgen-independence and osseous metastasis. *Prostate*. 2000;44(2):91–103.
18. Taylor BS, et al. Integrative genomic profiling of human prostate cancer. *Cancer Cell*. 2010;18(1):11–22.
19. Grytli HH, Fagerland MW, Fosså SD, Taskén KA, Håheim LL. Use of β-blockers is associated with prostate cancer-specific survival in prostate cancer patients on androgen deprivation therapy [published online ahead of print July 20, 2012]. *Prostate*. doi:10.1002/pros.22564.
20. Nagmani R, Pasco DS, Salas RD, Feller DR. Evaluation of beta-adrenergic receptor subtypes in the human prostate cancer cell line-LNCaP. *Biochem Pharmacol*. 2003;65(9):1489–1494.
21. Samama P, Pei G, Costa T, Cotecchia S, Lefkowitz RJ. Negative antagonists promote an inactive conformation of the beta 2-adrenergic receptor. *Mol Pharmacol*. 1994;45(3):390–394.
22. Sastry KS, Smith AJ, Karpova Y, Datta SR, Kulik G. Diverse antiapoptotic signaling pathways activated by vasoactive intestinal polypeptide, epidermal growth factor, and phosphatidylinositol 3-kinase in prostate cancer cells converge on BAD. *J Biol Chem*. 2006;281(30):20891–20901.
23. She QB, Solit DB, Ye Q, O'Reilly KE, Lobo J, Rosen N. The BAD protein integrates survival signaling by EGFR/MAPK and PI3K/Akt kinase pathways in PTEN-deficient tumor cells. *Cancer Cell*. 2005; 8(4):287–297.
24. Zha J, Harada H, Yang E, Jockel J, Korsmeyer SJ. Serine phosphorylation of death agonist BAD in response to survival factor results in binding to 14-3-3 not BCL-X(L). *Cell*. 1996;87(4):619–628.
25. Harada H, et al. Phosphorylation and inactivation of BAD by mitochondria-anchored protein kinase A. *Mol Cell*. 1999;3(4):413–422.
26. Cole SW, Sood AK. Molecular pathways: beta-adrenergic signaling pathways in cancer. *Clin Cancer Res*. 2012;18(5):1201–1206.
27. Shaywitz AJ, Greenberg ME. CREB: a stimulus-induced transcription factor activated by a diverse array of extracellular signals. *Annu Rev Biochem*. 1999;68:821–861.
28. Guo M, et al. Cytokines regulate beta-2-adrenergic receptor responsiveness in airway smooth muscle via multiple PKA- and EP2 receptor-dependent mechanisms. *Biochemistry*. 2005;44(42):13771–13782.
29. Ellwood-Yen K, et al. Myc-driven murine prostate cancer shares molecular features with human prostate tumors. *Cancer Cell*. 2003;4(3):223–238.
30. Hoffman B, Liebermann DA. Apoptotic signaling by c-MYC. *Oncogene*. 2008;27(50):6462–6472.
31. So AI, Hurtado-Coll A, Gleave ME. Androgens and prostate cancer. *World J Urol*. 2003;21(5):325–337.
32. Scattoni V, et al. Pathological changes of high-grade prostatic intraepithelial neoplasia and prostate cancer after monotherapy with bicalutamide 150 mg. *BJU Int*. 2006;98(1):54–58.
33. Isaacs JT, Lundmo PI, Berges R, Martikainen P, Kyprianou N, English HF. Androgen regulation of programmed death of normal and malignant prostatic cells. *J Androl*. 1992;13(6):457–464.
34. Nickerson T, Pollak M. Bicalutamide (Casodex)-induced prostate regression involves increased expression of genes encoding insulin-like growth factor binding proteins. *Urology*. 1999;54(6):1120–1125.
35. Danial NN. BAD: undertaker by night, candyman by day. *Oncogene*. 2008;7(suppl 1):S53–S70.
36. Feldman BJ, Feldman D. The development of androgen-independent prostate cancer. *Nat Rev Cancer*. 2001;1(1):34–45.
37. Kasbohm EA, et al. Androgen receptor activation by G(s) signaling in prostate cancer cells. *J Biol Chem*. 2005;280(12):11583–11589.
38. Sadar MD. Androgen-independent induction of prostate-specific antigen gene expression via cross-talk between the androgen receptor and protein kinase A signal transduction pathways. *J Biol Chem*. 1999;274(12):7777–7783.
39. Blok LJ, de Ruiter PE, Brinkmann AO. Forskolin-induced dephosphorylation of the androgen receptor impairs ligand binding. *Biochemistry*. 1998; 37(11):3850–3857.
40. Fu M, et al. The androgen receptor acetylation site regulates cAMP and AKT but not ERK-induced activity. *J Biol Chem*. 2004;279(28):29436–29449.
41. Selye H. *The Stress of Life*. New York, New York, USA: McGraw-Hill; 1956.
42. Ben Eliyahu S, Page GG, Schleifer SJ. Stress, NK cells, and cancer: Still a promissory note. *Brain Behav Immun*. 2007;21(7):881–887.
43. Sloan EK, et al. The sympathetic nervous system induces a metastatic switch in primary breast cancer. *Cancer Res*. 2010;70(18):7042–7052.
44. Thaker PH, Sood AK. Neuroendocrine influences on cancer biology. *Semin Cancer Biol*. 2008; 18(3):164–170.
45. Ramberg H, et al. Hormonal regulation of beta2-adrenergic receptor level in prostate cancer. *Prostate*. 2008;68(10):1133–1142.
46. Gousse A, Yoshida M, Weiss RM, Latifpour J. Beta adrenergic receptor alterations in diabetic rat prostate: effects of insulin and dietary myoinositol. *Prostate*. 1991;19(2):121–131.
47. Cao L, et al. Environmental and genetic activation of a brain-adipocyte BDNF/leptin axis causes cancer remission and inhibition. *Cell*. 2010;142(1):52–64.
48. Poyet P, Gagne B, Labrie F. Characteristics of the beta-adrenergic stimulation of adenylate cyclase activity in rat ventral prostate and its modulation by androgens. *Prostate*. 1986;9(3):237–245.
49. Krajewska M, et al. Elevated expression of inhibitor of apoptosis proteins in prostate cancer. *Clin Cancer Res*. 2003;9(13):4914–4925.
50. Royuela M, Arenas MI, Bethencourt FR, Sanchez-Chapado M, Fraile B, Paniagua R. Immunoexpressions of p21, Rb, mcl-1 and bad gene products in normal, hyperplastic and carcinomatous human prostates. *Eur Cytokine Netw*. 2001;12(4):654–663.
51. Yu J, et al. Integrative genomics analysis reveals silencing of beta-adrenergic signaling by polycomb in prostate cancer. *Cancer Cell*. 2007;12(5):419–431.
52. Prowatke I, et al. Expression analysis of imbalanced genes in prostate carcinoma using tissue microarrays. *Br J Cancer*. 2007;96(1):82–88.
53. Koh CM, Bieberich CJ, Dang CV, Nelson WG, Yegnasubramanian S, De Marzo AM. MYC and prostate cancer. *Genes Cancer*. 2010;1(6):617–628.
54. Massie MJ. Prevalence of depression in patients with cancer. *J Natl Cancer Inst Monogr*. 2004;(32):57–71.
55. Shahzad MM, et al. Stress effects on FosB- and interleukin-8 (IL8)-driven ovarian cancer growth and metastasis. *J Biol Chem*. 2010;285(46):35462–35470.
56. Sood AK, et al. Adrenergic modulation of focal adhesion kinase protects human ovarian cancer cells from anoikis. *J Clin Invest*. 2010;120(5):1515–1523.
57. Hara MR, et al. A stress response pathway regulates DNA damage through beta2-adrenoreceptors and beta-arrestin-1. *Nature*. 2011;477(7364):349–353.
58. Feng Z, et al. Chronic restraint stress attenuates p53 function and promotes tumorigenesis. *Proc Natl Acad Sci U S A*. 2012;109(18):7013–7018.
59. Datta SR, et al. Akt phosphorylation of BAD couples survival signals to the cell- intrinsic death machinery. *Cell*. 1997;91(2):231–241.
60. Kulik G, Klippel A, Weber MJ. Antiapoptotic signalling by the insulin-like growth factor I receptor, phosphatidylinositol 3-kinase, and Akt. *Mol Cell Biol*. 1997;17(3):1595–1606.
61. Baiz D, et al. Synthesis and characterization of a novel prostate cancer-targeted phosphatidylinositol-3-kinase inhibitor prodrug. *J Med Chem*. 2012; 55(18):8038–8046.